SCIENTIFIC REPORTS
nature research

OPEN

Masking Phosphate with Rare-Earth Elements Enables Selective Detection of Arsenate by Dipycolylamine-Zn^{II} Chemosensor

Nutsara Mekjinda[1], Supho Phunnarungsi[2], Vithaya Ruangpornvisuti[2], Raymond J. Ritchie[3], Itaru Hamachi[4], Akio Ojida[5*] & Jirarut Wongkongkatep[1*]

Functional reassessment of the phosphate-specific chemosensors revealed their potential as arsenate detectors. A series of dipicolylamine (Dpa)-Zn^{II} chemosensors were screened, among which acridine Dpa-Zn^{II} chemosensor showed the highest capability in sensing arsenate. The presence of excess Zn^{II} improved sensitivity and strengthened the binding between acridine Dpa-Zn^{II} complex to arsenate as well as phosphate. However, due to their response to phosphate, these sensors are not suited for arsenate detection when phosphate is also present. This study demonstrated for the first time that rare-earth elements could effectively mask phosphate, allowing the specific fluorescence detection of arsenate in phosphate-arsenate coexisting systems. In addition, detection of arsenate contamination in the real river water samples and soil samples was performed to prove its practical use. This sensor was further employed for the visualization of arsenate and phosphate uptake in vegetables and flowering plants for the first time, as well as in the evaluation of a potent inhibitor of arsenate/phosphate uptake.

Arsenic is a chemical analog of phosphorus that belongs to the same periodic group and shares a number of similarities with phosphorus, including the same number of valence electrons and nearly identical electronegativity (2.18 for As and 2.19 for P)[1]. Phosphorus- and arsenic-derived oxoanions, importantly inorganic phosphate (Pi) and arsenate, also exhibit similar properties[2], such as tetrahedral geometry and close bond lengths (1.69A° and 1.52A° for arsenate ($HAsO_4^-$) and phosphate (HPO_4^-), respectively)[3] Their acid counterparts also have similar dissociation constants (pK_a 2.26, 6.76, and 11.29 for the arsenic acid compared with 2.16, 7.21, and 12.32 for phosphoric acid)[1], thus possessing the same net charge acr.oss pH values. These salient physiochemical similarities to phosphate make arsenate highly toxic to humans. In addition, arsenate is a confirmed carcinogen and the most significant chemical contaminant in drinking-water worldwide[4].

Detection of arsenate has been conventionally conducted by atomic absorption spectrometry (AAS) and inductively coupled plasma mass spectrometry (ICPMS)[5–10]. However, the techniques require laborious sample preparation and cannot be employed to visualize biological phenomena in *situ*. To overcome this problem, several arsenate-specific chemosensors were developed[11–15], but they were only compatible with organic or aqueous-organic media and can be unstable in water[16]. Egdal *et al.* (2009) reported the divanadyl complex which was able to selectively bind to arsenate over Pi in aqueous solution, but it was optimal at a slightly acidic pH (pH = 3)[17]. Therefore, for the purpose of arsenate detection in drinking water and biological systems, a chemosensor that is stable in neutral aqueous solution would be more attractive.

Because of the significant roles in biological and environmental systems of the Pi anion, considerable efforts have been devoted to developing methods to detect Pi. These include the well-known colorimetric methods such as molybdenum blue[18–21] and small molecule-based fluorescence chemosensors, which show promise as

[1]Department of Biotechnology, Faculty of Science, Mahidol University, Rama 6 Road, Bangkok, 10400, Thailand. [2]Department of Chemistry, Faculty of Science, Chulalongkorn University, Phayathai Road, Pathumwan, Bangkok, 10330, Thailand. [3]Tropical Plant Biology, Faculty of Technology and Environment, Prince of Songkla University Phuket, Vichitsongkram Road, Kathu, Phuket, 83120, Thailand. [4]Department of Synthetic Chemistry and Biological Chemistry, Faculty of Engineering, Kyoto University, Katsura, Kyoto, 615-8510, Japan. [5]Graduate School of Pharmaceutical Sciences, Kyushu University, 3-1-1 Maidashi, Higashi-ku, Fukuoka, 812-8582, Japan. *email: ojida@phar.kyushu-u.ac.jp; jirarut.chu@mahidol.ac.th

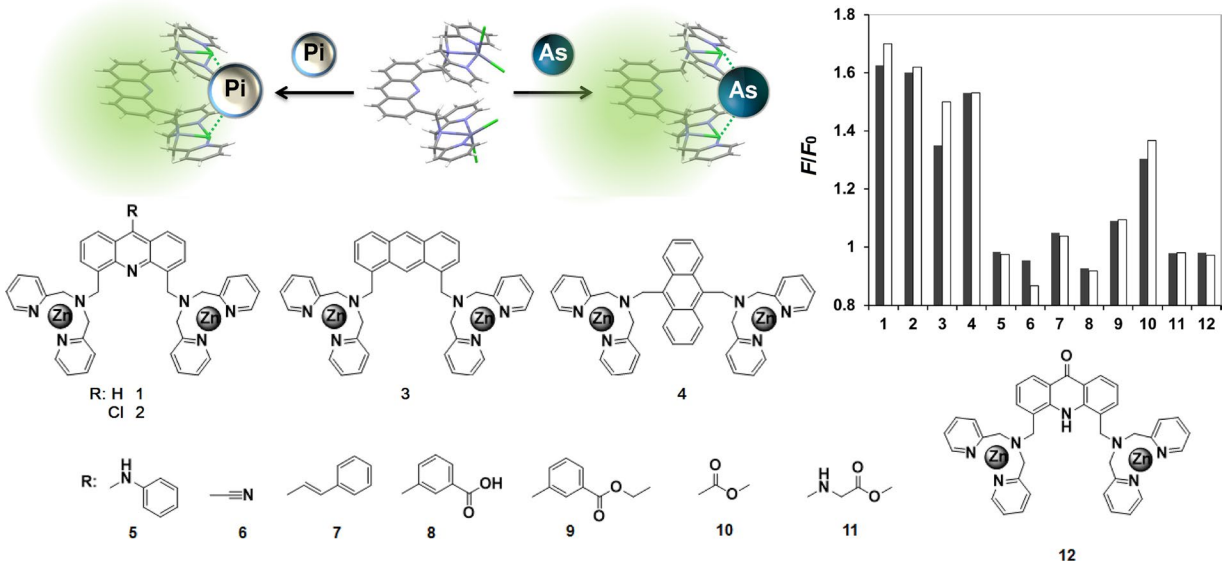

Figure 1. Schematic illustration of the binuclear Dpa-Zn^{II} complex library for fluorescence sensing of arsenate (As) and inorganic phosphate (Pi) and their chemical structures. Bar graph represents the fluorescence change (F/F_0) of each compound (5 μM) upon addition of 15 μM of arsenate (gray) or Pi (white).

analytical tools for the exploration of Pi-related biological processes[22–24]. Compared with the enormous number of reports relating to the detection of Pi, reports of fluorometric arsenate measurement are scant[25]. Owing to their similar chemical properties, we hypothesized that several sensing systems for Pi anion are also applicable to the detection of arsenate anion. We therefore examined the existing chemical sensors developed for Pi detection, as a novel sensing scaffold for arsenate detection. Our developed binuclear zinc complex served as the first turn-on fluorescence molecular sensor for arsenate under neutral aqueous solution[11–15]. However in the arsenate-phosphate coexisting environment, a novel strategy which can suppress the Pi detection while maintaining the arsenate sensing capability would be definitely required. We report a novel strategy of using rare-earth elements to mask Pi and promote specific fluorescence detection of arsenate by small-molecule chemosensors. We found that in the presence of rare-earth elements the binuclear zinc complex exhibited another function as the turn-on fluorescence sensor specific to arsenate with reduced sensitivity toward Pi. The developed sensing system was successfully employed for determination of arsenate contamination in real river water and soil samples contained natural Pi. The aquatic vascular plant *Wolffia* was used as the model plant for the imaging study. The ability to find arsenate contamination in vegetables using a fluorescence microscopy is potentially very important for public health reasons and demonstrated for the first time in this study.

Result and Discussion

Arsenate sensing performance. The binuclear Dpa-Zn^{II} moieties have been studied extensively as an effective binding motif of Pi and its derivatives (Fig. 1)[26]. These complexes have been designed to imitate the binding sites of metalloenzymes, in which the substrate Pi is recognized through reversible coordination to one or more Zn^{II} ions in the binding pocket[27]. Based on density functional theory (DFT) calculations with the B3LYP/6-31 G(d) level of theory, almost similar binding properties of Dpa-Zn^{II} moiety toward arsenate and Pi were found. All the optimized structures of Dpa-Zn^{II} complex after binding to arsenate and Pi, their hydrogen-bond distances, Gibbs free energy of complexations were calculated (see Supplementary Fig. S1, Tables S1 and S2). The results from DFT calculations clearly revealed negligible difference in the binding mode of **1** toward arsenate and Pi. The screening experiment also showed that each of the 12 Dpa-Zn^{II} compounds in our library responded similarly to addition of arsenate and Pi, indicating that these chemosensors were capable of sensing both anionic species (Fig. 1).

The compound **1**, in which acridine fluorophore was conjugated to two Dpa-Zn^{II} moieties, showed approximately 1.6-fold increase in fluorescence emission - the highest among the library compounds tested (Fig. 1). It also displayed a hypochromic shift of the maximum emission from 472 nm to 444 nm in 10 mM HEPES buffer (pH 7.2) upon addition of arsenate and Pi (Fig. 2). These changes were similar to the result that Yoon *et al.* (2007) reported this sensor as a sensing motif for Pi[26]. When Zn^{II} was supplied in excess, the fluorescence intensification of the **1** upon arsenate addition was significantly increased from 3-fold to 7-fold as shown in Fig. 2b and summarized in Table 1. Similar phenomenon was observed in the case of Pi addition (Fig. 2d).

In aqueous HEPES buffer (pH 7.2), the observed emission maximum (see Supplementary Fig. S2) and the shape of the UV/Vis spectrum (see Supplementary Fig. S3) indicated that **1** existed predominantly as a mononuclear Zn^{II} complex with coordination between the Zn^{II} ion and the acridine nitrogen atom. The complexation constants of the first and second Zn^{II} ions of **1** in aqueous HEPES buffer were determined by the Zn^{II} titration experiments to be $>10^7$ and $3.3 \times 10^4\ M^{-1}$, respectively, suggesting that the second Zn^{II} ion would not be fully complexed at low micromolar concentrations, which was in good agreement to the case of **2** reported previously[22].

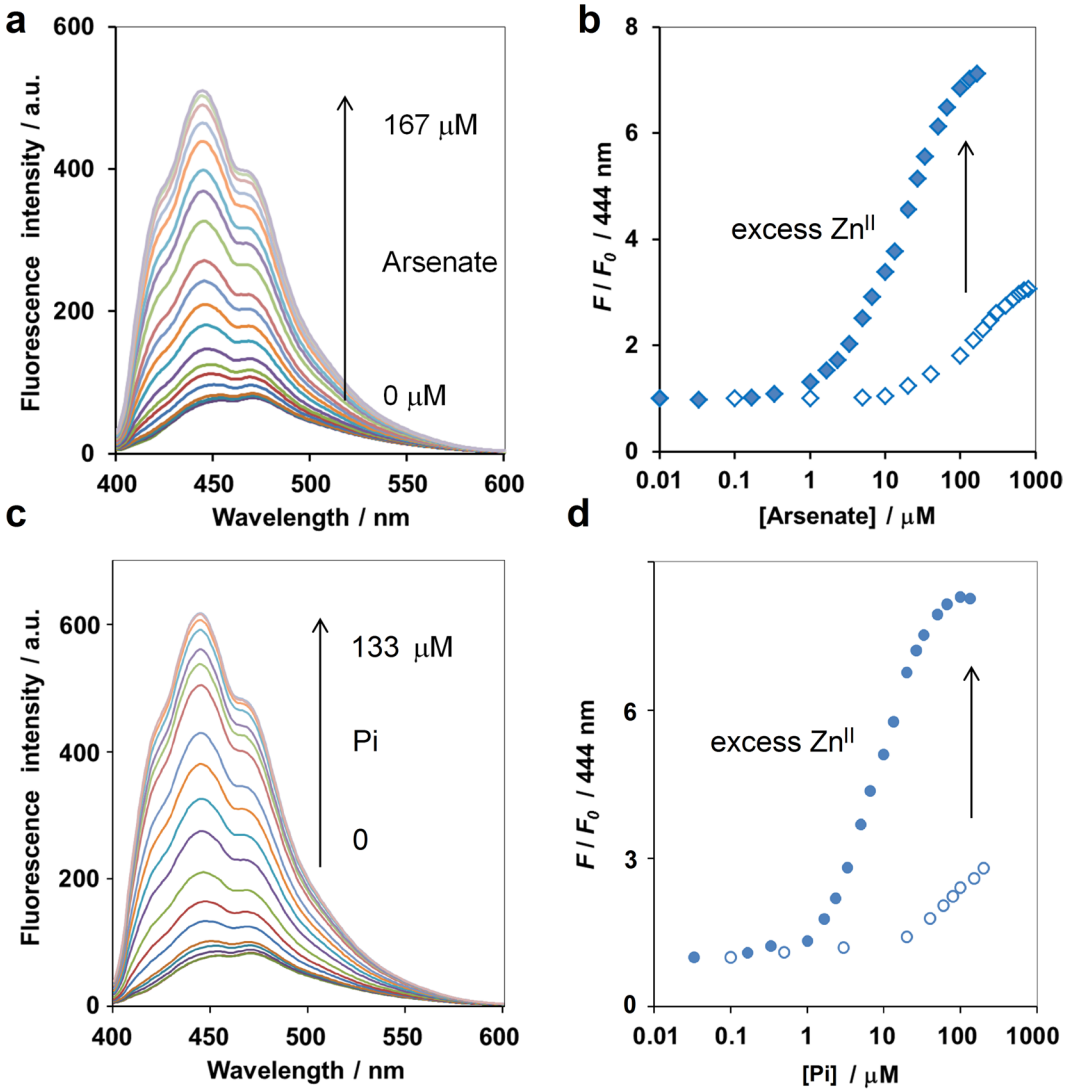

Figure 2. Fluorescence emission of **1** (5 μM) upon addition of arsenate (**a**) and Pi (**c**) in the presence of 0.1 mM $ZnSO_4$ and changes in the emission intensity at 444 nm of **1** (5 μM) upon addition of arsenate (**b**) and Pi (**d**) with (filled symbol) and without (empty symbol) addition of 0.1 mM $ZnSO_4$. Measurement condition: 10 mM HEPES buffer (pH 7.2), 25 °C. λ_{ex} 359 nm.

Sensor	$\lambda_{ex}/\lambda_{em}$ (nm)	Arsenate		Pi	
		K_{app} (M^{-1})	F_{max}/F_0	K_{app} (M^{-1})	F_{max}/F_0
1	359/444	2.7×10^5	7.1	1.4×10^6	8.3
2	368/451	8.3×10^5	3.4	4.2×10^5	4.4
3	370/421	2.2×10^5	1.6	5.5×10^5	1.6
4	380/435	1.2×10^4	2.0	3.6×10^4	2.6

Table 1. Summary of the Apparent Binding Constant (K_{app}, M^{-1}) and the Maximum Relative Emission Intensity (F_{max}/F_0) of the Selected Sensors under Excess Zn^{II} Condition Tested in this Study.

The 20-equivalent excess of Zn^{II} to **1** supplied in this study could offset the low value of the complexation constant of the second zinc ion and enable the formation of binuclear **1** complex capable of arsenate sensing. Addition of excess Zn^{II} also suppressed the fluorescence background of **1** by 44%. As a result, the fluorescence increase of **1** upon arsenate addition was as high as 7-fold in the presence of excess Zn^{II} compared with only 3-fold when Zn^{II} was not in excess (Fig. 2b). Thus, the presence of excess Zn^{II} could drastically increase the sensitivity of **1** for both arsenate and Pi detection, as well as decrease the lower detection limit of **1** toward arsenate from 10 to 4 μM.

The increase in fluorescence emission and the blue shift of **1** due to arsenate were almost identical to those obtained with Pi addition (Fig. 2), indicating that both arsenate and Pi may interact with **1** through a similar

mechanism. The Job plot between **1** and arsenate revealed 1:1 stoichiometry (see Supplementary Fig. S4), similar to that of **1** and Pi, and in good agreement with the previous report[26]. From the fluorescence titration under excess Zn^{II} condition, the apparent binding constant (K_{app}) between **1** and arsenate was $2.7 \times 10^5\,M^{-1}$ as determined by the least-square curve-fitting method (Table 1), while the corresponding value for Pi binding was calculated to be $1.4 \times 10^6\,M^{-1}$. Yoon *et al.* (2007) reported the K_{app} between **1** and Pi to be $9.34 \times 10^4\,M^{-1}$ −15-fold lower than the K_{app} calculated under the excess Zn^{II} condition used in this study[26]. The observed difference in K_{app} suggested that the presence of excess Zn^{II} not only enhanced the sensitivity of the fluorescence detection, but also strengthened the binding affinity between **1** and the target anion. Possibly, this may be because coordination of the second Zn^{II} is required to poise the conformation of the binuclear **1** complex for arsenate and Pi sensing.^{1}H NMR spectra suggested the possibility of the coordination between acridine nitrogen atom and the first Zn^{II} but such coordination was cancelled when the second Zn^{II} was fully coordinated with the Dpa moieties (see Supplementary Fig. S5).

The selectivity test confirmed the high sensitivity of **1** toward arsenate and Pi, but not toward arsenite and other anions commonly found in nature such as chloride, bromide, iodide, sulfate, acetate, and inorganic pyrophosphate (see Supplementary Fig. S6). Such selectivity was in good agreement with the previous reports of Hamachi *et al.*[22] and Yoon *et al.*[26]. However, while this selectivity against other ions was desirable for arsenate detection in real environmental samples, the inability of **1** to distinguish between Pi and arsenate would still be problematic due to the abundance of the former in nature. Therefore, a novel strategy to preclude Pi binding is essential to improve the accuracy and precision of arsenate detection under the Pi-abundant conditions.

Masking with rare-earth element. As rare-earth elements were reported to show stronger affinity toward Pi than arsenate, we sought to test their efficacy as novel masking agents of Pi in 100% aqueous solution and at neutral pH. Yttrium (Y^{III}) exhibits an approximately 100-fold difference in K_{sp} between YPO_4 and $YAsO_4$ (pK_{sp} are 24.76 and 22.60, respectively)[28,29]. Therefore, Y^{III} was employed as a new type of masking agent of Pi for detection of arsenate using **1**. The rationale is that when both arsenate and Pi are present, Y^{III} will selectively form aggregate with Pi while arsenate will remain soluble and can be detected by the sensor (Fig. 3a).

In the absence of Y^{III}, chemosensor **1** was more selective towards Pi than arsenate. However, when 25 μM of Y^{III} was included, **1** became more specific to arsenate than Pi. The higher concentration of Y^{III} suppressed the F/F_0 of **1** toward Pi at the baseline while it slightly lowered the fluorescence response of **1** to arsenate (Fig. 3b). At fixed 25 μM of Y^{III}, addition of Pi up to nearly 25 μM did not raise the fluorescence level of **1** from the baseline. This result indicated that Y^{III} and Pi formed a nanostructure with 1:1 stoichiometry, leaving free Pi at a concentration below the detection limit of **1** (i.e. below 1 μM Pi). Addition of Pi at concentration higher than 25 μM induced an increase in F/F_0 of **1**, suggesting that the free Y^{III} ion had been depleted due to formation of YPO_4 and could no longer sequester the oncoming Pi. Increasing in the concentration of Y^{III} allowed more Pi to be effectively masked (Fig. 3c), indicating that this masking effect strongly depended on the concentration of Y^{III}. However, at high concentration of Y^{III}, the masking capacity of Y^{III} slightly dropped, as 100 μM of Y^{III} could mask Pi only up to approximately 75 μM (Fig. 3c). This deviation requires further investigation.

When arsenate and Pi were simultaneously present, Y^{III} did not appear to mask arsenate, as indicated by approximately 6-fold fluorescence enhancement upon addition of arsenate to the aqueous solution containing **1** and 25 μM Pi. In the absence of Y^{III}, 25 μM of Pi (5 equivalents to **1**) was able to saturate **1** and resulted in the lack of fluorescence sensing capability upon addition of arsenate (Fig. 3d). Dynamic light scattering (DLS) also confirmed that mixing Y^{III} with Pi led to the formation and growth of YPO_4 nanostructures, which reached the final size of 451 ± 87 nm, while no growth of $YAsO_4$ was observed under a similar condition (Fig. 3e). Taken together, these results demonstrated for the first time that the formation of YPO_4 nanoaggregate is an effective Pi masking strategy in the arsenate-Pi coexisting system.

In addition to Yttrium, other rare-earth elements including Lanthanum (La), Cerium (Ce) and Lutetium (Lu) exhibited a similar masking effect when tested under the same condition (Fig. 4a). The fluorescence response of **1** toward arsenate was unaffected by addition of Y^{III}, La^{III}, Ce^{III} and Lu^{III}, suggesting that rare-earth elements did not disturb the sensor's arsenate detection capability (Fig. 4b). The values of K_{app} between **1** and arsenate in the presence of rare-earth elements ranged from $3.2 \times 10^4\,M^{-1}$ in the case of Lu^{III} to $5.1 \times 10^4\,M^{-1}$ in the case of Ce^{III} (Table 2) and was not significantly different among species of rare-earth elements tested. In addition, rare-earth elements could still effectively mask Pi when the chemosensor was changed to **2** and **3**, suggesting that this strategy was relatively independent of the types of probe. However, under high concentration of Y^{III} (150 μM), arsenate binding was weakened and the K_{app} between **1** and arsenate diminished to $3.0 \times 10^3\,M^{-1}$, an order of magnitude less than the K_{app} at low concentration of Y^{III} (25 μM) (Table 2). Collectively, these results suggested that rare-earth elements were generally effective in masking Pi without compromising arsenate-sensing ability, although at excessive concentrations they could be detrimental to arsenate binding. While high Pi content can be found in the environmental samples, which may necessitate correspondingly high concentration of the masking agent, natural Pi contents in water resources and soil solutions rarely exceed 4 and 10 μM[30,31]. Therefore, 25 μM Y^{III} should be sufficient for effective masking of phosphate in analysis of normal environmental samples.

Detection of arsenate in the river water and soil samples. Tens millions of people in south and southeast Asia are considered to be at risk from consuming water that has unsafe arsenic levels. It has been suggested that arsenic is naturally released from near-surface, river-derived sediments and transported over centuries through the underlying aquifer back to the river[32,33]. Arsenate is a common form of arsenic usually found in water supplies[34]. Using **1** for detection of arsenate in environmental samples such as river water and soil was successfully demonstrated as shown in Fig. 5. This method also showed good linearity ($R^2 > 0.989$) when **1** was applied to the artificially spiked river water as well as the water-extractable portion of soil in a 96-well plate format. These results confirmed the utility of **1** in high-throughput arsenate detection in a complex environmental sample containing

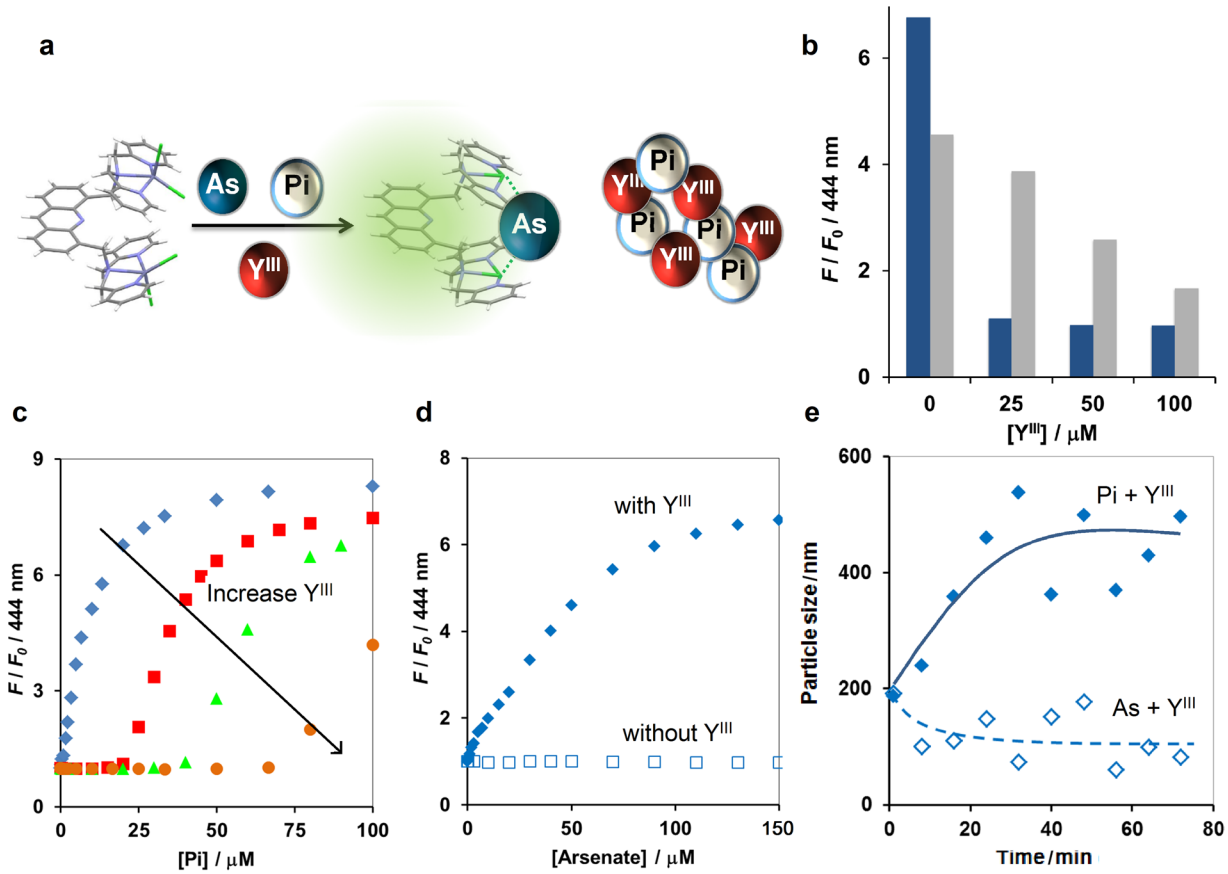

Figure 3. (**a**) Schematic illustration of masking with Y^{III} for detection of arsenate (As) in the presence of Pi. (**b**) Fluorescence change at 444 nm of **1** (5 μM) upon addition of 20 μM arsenate (gray) or Pi (blue) at different concentration of Y^{III}. (**c**) Fluorescence change at 444 nm of **1** (5 μM) upon addition of different concentration of Pi when Y^{III} was added at the concentrations of 0 (blue diamond), 25 (red square), 50 (green triangle) and 100 μM (brown circle). (**d**) Fluorescence sensing of arsenate using **1** (5 μM) in the presence (filled diamond) and absence (empty square) of 50 μM Y^{III} as a masking agent when Pi (25 μM) was present. Measurement condition: 10 mM HEPES buffer (pH 7.2), 0.1 mM $ZnSO_4$, 25 °C. λ_{ex} 359 nm. (**e**) Time-course DLS analysis of the nanoaggregates after equimolar of arsenate (empty symbol) or Pi (filled symbol) was added to the aqueous solution of Y^{III}.

natural Pi, which is a major interference for an accurate measurement of arsenate concentration in spectrophotometric analysis.

Bioimaging of arsenate and Pi in *Wolffia*. Arsenate accumulation in rice[9,35–38], fruit and flowering plants[39–41] is considered a major problem for consumers. It has been suggested that uptake of arsenate in plants relies on PHT phosphate transporters, a specific family of plant plasma membrane proteins[42–44], but the detailed mechanism has not yet been elucidated due to the lack of an appropriate visualization tool. The improved sensitivity of **1** upon excess Zn^{II} condition encouraged us to apply this small-molecular probe for the bioimaging of arsenate and Pi in plant for the first time. *Wolffia* (*Wolffia arrhiza*), the flowering plant species consumed as a vegetable in South East Asia was selected as a model study. The bright blue color of **1**/arsenate and **1**/Pi complex were detected only when arsenate or Pi was introduced to the *Wolffia* as clearly shown in Fig. 6a. Bright fluorescence from **1**/arsenate and **1**/Pi colocalized with the signal from toluidine blue O staining, suggesting that the complex may be located at the carboxylated polysaccharide accumulated in the cell wall[45] (see Supplementary Fig. S7). The images further revealed that the depletion of Pi in *Wolffia* occurred faster than arsenate, as the bright fluorescence from **1**/Pi complex disappeared at 3 h post Pi addition, whereas the signal from **1**/arsenate remained for more than 3 h (Fig. 6b). Image analysis revealed that the signal arising from the arsenate-sensor complex exhibited the maximum intensity of 104.02 ± 2.02 at one hour after incubation, then remained almost unchanged throughout 3 h of observation. However, the fluorescence emission from **1**/Pi achieved the maximum intensity of 103.61 ± 1.07 after two hours before decreasing to 48.44 ± 0.96 at the 3rd hour (Fig. 6b). Addition of Y^{III} exhibited the higher masking efficiency toward Pi rather than As (Fig. 6), indicating that rare-earth element can be employed for masking of Pi under imaging analysis. Inhibition of arsenate uptake could also be visualized with **1**, as inclusion of photonophore, 2,4-dinitrophenol (DNP) and diethylstilbestorol (DESS), a reported inhibitor of PHT1 phosphate transporter[42], significantly decreased the observed fluorescence intensity (Fig. 6a, lower panel). This finding strongly supported the hypothesis that arsenate acquisition depends on PHT1 phosphate

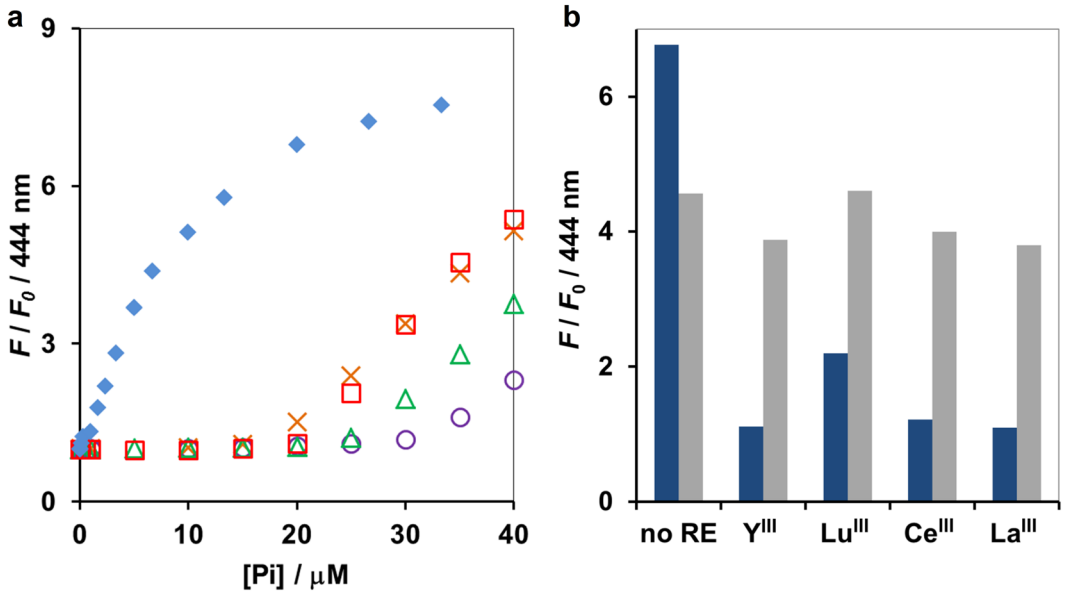

Figure 4. (**a**) Fluorescence change at 444 nm of **1** (5 μM) upon binding to Pi without (blue diamond) and with 25 μM of Y^{III} (red square), Lu^{III} (orange cross), Ce^{III} (green triangle), La^{III} (purple circle) as a masking agent. (**b**) The comparison of F/F_0 at 444 nm of **1** (5 μM) upon binding to 25 μM arsenate (gray) and Pi (blue) under 25 μM of each rare-earth element. Measurement condition: 10 mM HEPES buffer (pH 7.2), 0.1 mM $ZnSO_4$, 25 °C. λ_{ex} 359 nm.

Sensor	K_{app} (M^{-1})				
	Y^{III}		Ce^{III}	La^{III}	Lu^{III}
1[a]	[Y^{III}]				
	25 μM	3.8×10^4	5.1×10^4	4.4×10^4	3.2×10^4
	50 μM	1.4×10^4	—	—	—
	100 μM	8.3×10^3			
	150 μM	3.0×10^3			
2[b]	1.9×10^4		2.5×10^4	3.1×10^4	1.5×10^4
3[c]	1.8×10^4		3.2×10^4	2.1×10^4	1.5×10^4

Table 2. Summary of the Apparent Binding Constant (K_{app}, M^{-1}) of Selected Sensors toward Arsenate in the Presence of Rare-earth Elements. [a]Measurement condition: 5 μM **1**, 0.1 mM $ZnSO_4$, 10 mM HEPES (pH 7.2), 25 °C, λ_{ex} 359 nm. [b]Measurement condition: 50 μM **2**, 0.2 mM $ZnSO_4$, 200 μM rare-earth element, 10 mM HEPES (pH 7.2), 25 °C, λ_{ex} 368 nm. [c]Measurement condition: 5 μM **3**, 50 μM rare-earth element, 10 mM HEPES (pH 7.2), 25 °C, λ_{ex} 370 nm.

transporter[42]. Taken together, these results confirmed the utility of **1** in bioimaging and screening of inhibitors of both arsenate and Pi uptake in vegetable and flowering plants under physiological condition. Previously, conventional methods such as radioactive ^{31}P labeling or genetically encoded fluorescent protein have been employed to study arsenate and Pi uptake through PHT phosphate transporter family in live plants[46,47]. However, to the best of our knowledge, our work is the first to use a small-molecule sensor to study this physiological arsenate uptake process *in situ*. Our proposed method can be applied in high-throughput screening of arsenate uptake inhibitors, which will be useful to prevent arsenic contamination in the edible plants so that they are safer for human consumption.

Conclusion

In this study, we confirmed another function of some small molecular-based chemosensors consisting of Dpa-Zn^{II}, which have been reported as a Pi sensor, as a new sensing platform for arsenate and its applicability for visualization of both arsenate and Pi uptake in plants, and for inhibitor screening of the PHT1 transporter in vascular plants. High-throughput screening for a potent inhibitor which prevents arsenate uptake but does not disrupt Pi acquisition in plants could be performed easily using our newly proposed sensing platform to save consumers from ingestion of arsenic-polluted vegetables and fruits. We also demonstrated that the rare-earth masking strategy is a versatile method to suppress the interference of Dpa-Zn^{II} complex-based chemosensor by Pi and allow for specific arsenate detection, enables the sensing of arsenate in natural Pi-arsenate coexisting systems such as river water and soil samples. Because the arsenic contamination in environment is a spatial and temporal

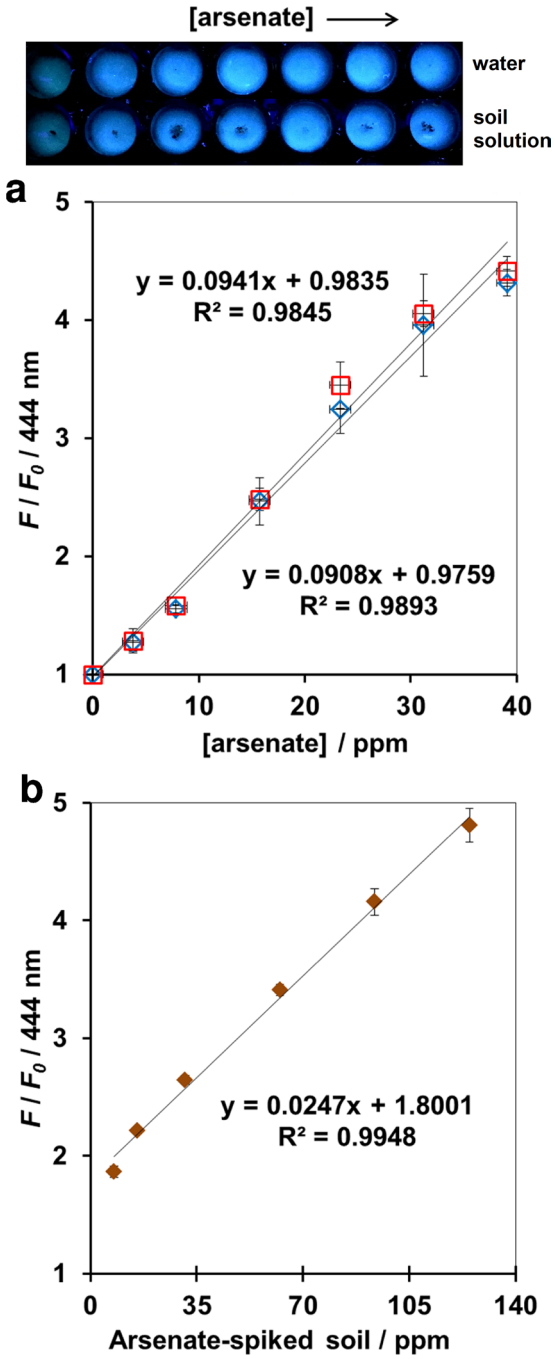

Figure 5. Fluorescence change at 444 nm of **1** (5 μM) when the following samples were added: (**a**) Na_2HAsO_4 spiked river water 1 (red square) or river water 2 (blue diamond); (**b**) water-extractable phase of soil spiked with Na_2HAsO_4. Measurement condition: 10 mM HEPES buffer (pH 7.2), 25 μM of $Y(CH_3COO)_3$, 0.1 mM $ZnSO_4$, 25 °C. λ_{ex} 359 nm. Three individual replicates were performed.

problem, a routine monitoring of arsenate level in water supplies in high-throughput manner would be another cost-effective strategy. While our study focused on Dpa-Zn^{II} sensors, we believe that this strategy is applicable to a broad range of highly sensitive chemical and bio-based sensors. Currently, for example, we are investigating the use of this masking strategy to convert a phosphate binding protein into an arsenate specific protein sensor, the outcome of which will be reported soon.

Methods

Chemicals and materials. All chemicals used in this work were of analytical reagent grade and used without further purification. Water used in all experiments was doubly distilled and purified by a Milli-Q system. Yttrium(III) acetate (99.9%, $(CH_3COO)_3Y{\cdot}4H_2O$), cerium(III) acetate ($Ce(CH_3COO)_3{\cdot}H_2O$), lanthanum(III) carbonate ($La_2(CO_3)_3$), lutetium acetate (99.9%, $(CH_3COO)_3Lu{\cdot}4H_2O$) and zinc acetate (99.9%,

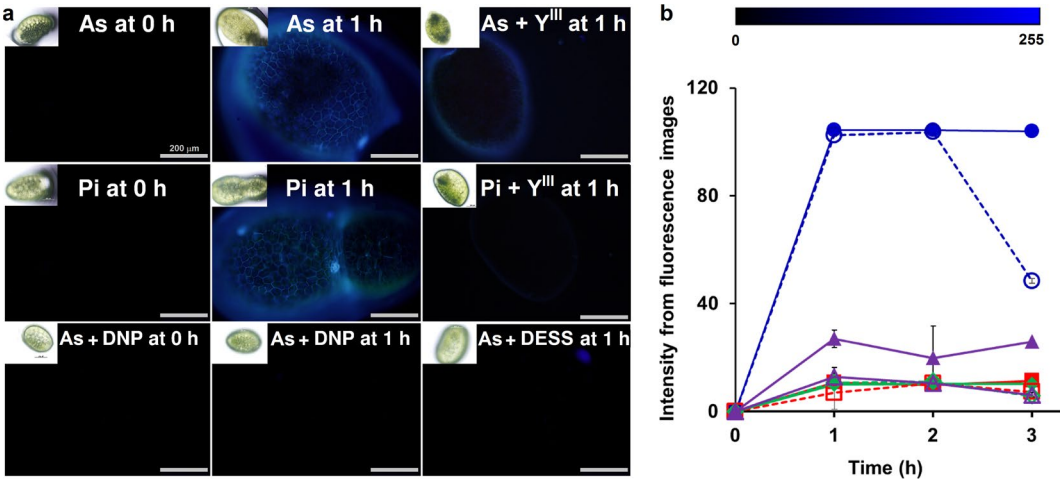

Figure 6. (**a**) Fluorescence images of *Wolffia arrhiza* when incubated with 1 mM Na_2HAsO_4 (As), 1 mM Na_2HPO_4 (Pi), and 0.1 mM DNP, 0.1 mM DESS or 0.05 mM Y^{III}. All specimens were subsequently incubated with 1 mM of **1**. Measurement condition: 20 mM $ZnSO_4$, 27 °C, exposure time 1/5.0. Scale bar: 200 μm. (**b**) Average intensities of fluorescence imaging of *Wolffia arrhiza* stained with **1** after treatment with 1 mM arsenate (filled symbols) and 1 mM Pi (empty symbols) in the absence (blue circle) and presence of 0.1 mM DNP (red square), 0.1 mM DESS (green diamond) or 0.05 mM Y^{III} (purple triangle). Data acquired from three individual replicates.

$(CH_3COO)_2Zn{\cdot}2H_2O$) were obtained from Wako (Osaka, Japan). Disodium hydrogen arsenate ($Na_2HAsO_4{\cdot}7H_2O$) and 4-(2-hydroxyethyl)-1-piperazineethanesulfonic acid (99.5%, HEPES) were purchased from Sigma-Aldrich (St. Loius, USA). Disodium hydrogen phosphate ($Na_2HPO_4{\cdot}12H_2O$) was acquired from Ajax Finechem (Taren Point, Australia). 2,4-dinitrophenol (DNP) and diethylstilbestorol (DESS) was purchased from Tokyo Chemical Industy (Tokyo, Japan). The synthesis of acridine skeleton chemical sensors **1**, **2** and anthracene skeleton chemical sensors **3**, **4** was performed following the literature[22,26,48]. Compounds **5–12** were obtained from Yoshifumi Miyahara's compound library of Hamachi Laboratory, Kyoto University.

Fluorescence measurement. A spectrofluorometer (Jasco FP 6500, Japan) was used for the determination of fluorescence intensity of the chemosensors upon binding with arsenate/phosphate. The excitation wavelength was determined based on the fluorometric property of each chemosensor. An automated microplate reader (TECAN, Spark 10 M, Switzerland) was used for the analysis in the 96-well plate format, particularly in the application of arsenate detection in soil and water samples. Fluorescence imaging was performed using fluorescence light microscope (Olympus BX51) with a camera set (Olympus PM10-SP) and UV filter. All spectra were recorded at 25 °C. Intensity of the acquired images was evaluated using Olympus cellSens Software dimension desktop 1.18.

Dynamic light scattering measurement. $Y(CH_3COO)_3$ was mixed with equimolar Na_2HPO_4 or Na_2HAsO_4 in a MilliQ purified water (resistivity <18 MΩ, conductivity 0.055 mS/cm) and filtered with 0.2 μm nylon membrane. The particle size of the nanoaggregate was recorded by Zetasizer Nano ZS (Marlvern Instrument, UK).

Preparation of soil and water samples. Water and soil samples used in this study were spiked with an appropriate concentration of disodium hydrogen arsenate (Na_2HAsO_4). Water artificially contaminated with arsenate was prepared by mixing the stock solution of disodium hydrogen arsenate (1.5 mM) with river water 1 and 2 which were collected in Bangkok, Thailand on 10 March 2018. Preparation of arsenic-contaminated soil sample (1.0 g) was performed by spiking the sandy loam soil (surface soil collected from Mahidol University, Phayathai campus, Bangkok Thailand) with arsenate and incubated at 25 °C for 3 days. Soil samples were then suspended in a MilliQ deionized water (10 mL) for 1 h and centrifuged (12,000 × g at 15 min) to obtain a clear supernatant as a water-extractable fraction of soil.

Preparation of *Wolffia* sample. *Wolffia* (*Wolffia arrhiza*) was commercially available from a local market in Bangkok, Thailand and grown in exterior tubs in commercial NPK medium with the pH adjusted to 5. Then it was soaked in 1 mM of disodium hydrogen arsenate or 1 mM disodium hydrogen phosphate without and with 0.1 mM DNP and DESS for 0, 1, 2 and 3 h at 27 °C. Then, the sample was further incubated in the solution of chemosensor **1** (1 mM) containing $ZnSO_4$ (20 mM) for 30 min in dark at 27 °C. The incubated *Wolffia* was transferred to a concave glass slide for fluorescence imaging.

Received: 25 November 2019; Accepted: 3 February 2020;
Published online: 14 February 2020

References

1. Lide, D. R. CRC Handbook of chemistry and physics, Internet Version 2005. **128**, 5585–5585, https://doi.org/10.1021/ja059868l (2006).
2. Elias, M. *et al*. The molecular basis of phosphate discrimination in arsenate-rich environments. *Nature* **491**, 134–137, https://doi.org/10.1038/nature11517 (2012).
3. Kish, M. M. & Viola, R. E. Oxyanion specificity of aspartate-β-semialdehyde dehydrogenase. *Inorg. Chem.* **38**, 818–820, https://doi.org/10.1021/ic981082j (1999).
4. IARC. Arsenic, metals, fibers, and dusts. *Monogr. Eval. Carcinog. Risks Hum.* **100**, 41–93 (2012).
5. Matoušek, T., Wang, Z., Douillet, C., Musil, S. & Stýblo, M. Direct speciation analysis of arsenic in whole blood and blood plasma at low exposure levels by hydride generation-cryotrapping-inductively coupled plasma mass spectrometry. *Anal. chem.* **89**, 9633–9637, https://doi.org/10.1021/acs.analchem.7b01868 (2017).
6. Kalman, D. A. *et al*. Occurrence of trivalent monomethyl arsenic and other urinary arsenic species in a highly exposed juvenile population in Bangladesh. *J. Expo. Sci. Environ. Epidemiol.* **24**, 113–120, https://doi.org/10.1038/jes.2013.14 (2014).
7. Stiboller, M., Raber, G., Gjengedal, E. L. F., Eggesbo, M. & Francesconi, K. A. Quantifying inorganic arsenic and other water-soluble arsenic species in human milk by HPLC/ICPMS. *Anal. Chem.* **89**, 6265–6271, https://doi.org/10.1021/acs.analchem.7b01276 (2017).
8. Musil, S., Matousek, T., Currier, J. M., Styblo, M. & Dedina, J. Speciation analysis of arsenic by selective hydride generation-cryotrapping-atomic fluorescence spectrometry with flame-in-gas-shield atomizer: achieving extremely low detection limits with inexpensive instrumentation. *Anal. Chem.* **86**, 10422–10428, https://doi.org/10.1021/ac502931k (2014).
9. Banerjee, M. *et al*. High arsenic in rice is associated with elevated genotoxic effects in humans. *Sci. Rep.* **3**, 2195, https://doi.org/10.1038/srep02195 (2013).
10. Alam, M. Z. *et al*. Arsenic accumulation in lentil (*Lens culinaris*) genotypes and risk associated with the consumption of grains. *Sci. Rep.* **9**, 9431, https://doi.org/10.1038/s41598-019-45855-z (2019).
11. Dey, S., Sarkar, S., Maity, D. & Roy, P. Rhodamine based chemosensor for trivalent cations: Synthesis, spectral properties, secondary complex as sensor for arsenate and molecular logic gates. *Sens. Actuators. B. Chem.* **246**, 518–534, https://doi.org/10.1016/j.snb.2017.02.094 (2017).
12. Banerjee, A. *et al*. Visible light excitable fluorescence probe and its functionalized merrifield polymer: selective sensing and removal of arsenate from real samples. *RSC Adv.* **4**, 3887–3892, https://doi.org/10.1039/c3ra45362f (2014).
13. Sahana, A. *et al*. Fluorescence sensing of arsenate at nanomolar level in a greener way: naphthalene based probe for living cell imaging. *Chem. Commun.* **49**, 7231–7233, https://doi.org/10.1039/c3cc43211d (2013).
14. Dolai, M., Alam, R., Katarkar, A., Chaudhuri, K. & Ali, M. Oxime based selective fluorescent sensor for arsenate ion in a greener way with bio-imaging application. *Anal. Sci.* **32**, 1295–1300, https://doi.org/10.2116/analsci.32.1295 (2016).
15. Lohar, S. *et al*. Antipyrine based arsenate selective fluorescent probe for living cell imaging. *Anal. Chem.* **85**, 1778–1783, https://doi.org/10.1021/ac3031338 (2013).
16. Liu, Y. & Trogler, W. C. Comment on 'Fluorescence sensing of arsenate at nanomolar level in a greener way: naphthalene based probe for living cell imaging'. *Chem. Commun.* **51**, 14775–14777, https://doi.org/10.1039/c5cc02494c (2015).
17. Egdal R. K. *et al*. Selective recognition and binding of arsenate over phosphate. *Dalton Trans.*, 9718–9721, https://doi.org/10.1039/b918143c (2009).
18. Mezei, G. Incarceration of one or two phosphate or arsenate species within nanojars, capped nanojars and nanohelicages: helical chirality from two closely-spaced, head-to-head PO_4^{3-} or AsO_4^{3-} ions. *Chem. Commun.* **51**, 10341–10344, https://doi.org/10.1039/c5cc03005f (2015).
19. Tsang, S., Phu, F., Baum, M. M. & Poskrebyshev, G. A. Determination of phosphate/arsenate by a modified molybdenum blue method and reduction of arsenate by $S_2O_4^{2-}$. *Talanta* **71**, 1560–1568, https://doi.org/10.1016/j.talanta.2006.07.043 (2007).
20. Müller, A. Bringing inorganic chemistry to life. *Chem. Comm.*, 803–806, https://doi.org/10.1039/b300207c (2003).
21. Stauffer, R. E. Determination of arsenic and phosphous compounds in groundwater with reduced molybdenum blue. *Anal. Chem.* **55**, 1205–1210, https://doi.org/10.1021/ac00259a006 (1983).
22. Ojida, A. *et al*. Design of dual-emission chemosensors for ratiometric detection of ATP derivatives. *Chem. Asian. J.* **1**, 555–563, https://doi.org/10.1002/asia.200600137 (2006).
23. Nadella, S. *et al*. Sensing of phosphates by using luminescent Eu^{III} and Tb^{III} complexes: application to the microalgal cell *Chlorella vulgaris*. *Chem. Eur. J.* **20**, 6047–6053, https://doi.org/10.1002/chem.201304664 (2014).
24. Meng, Q. *et al*. A new fluorescent chemosensor for highly selective and sensitive detection of inorganic phosphate (Pi) in aqueous solution and living cells. *RSC Adv.* **5**, 53189–53197, https://doi.org/10.1039/c5ra08712k (2015).
25. Ma, J., Sengupta, M. K., Yuan, D. & Dasgupta, P. K. Speciation and detection of arsenic in aqueous samples: a review of recent progress in non-atomic spectrometric methods. *Anal. Chim. Acta.* **831**, 1–23, https://doi.org/10.1016/j.aca.2014.04.029 (2014).
26. Lee, H. N. *et al*. Simple but effective way to sense pyrophosphate and inorganic phosphate by fluorescence changes. *Org. Lett.* **9**, 243–246, https://doi.org/10.1021/ol062685z (2007).
27. Gonzalez, D., Richez, M., Bergonzi, C., Chabriere, E. & Elias, M. Crystal structure of the phosphate-binding protein (PBP-1) of an ABC-type phosphate transporter from *Clostridium perfringens*. *Sci. Rep.* **4**, 6636, https://doi.org/10.1038/srep06636 (2014).
28. Firsching, F. H. & Brune, S. N. Solubility products of the trivalent rare-earth phosphates. *J. Chem. Eng. Data* **36**, 93–95, https://doi.org/10.1021/je00001a028 (1991).
29. Firsching, F. H. Solubility products of the trivalent rare-earth arsenates. *J. Chem. Eng. Data* **37**, 497–499, https://doi.org/10.1021/je00008a028 (1992).
30. Dokulil, M. T. & Teubner, K. In *Eutrophication: causes, consequences and control* (ed. Ansari, A. A., Gill, S. S., Lanza, G. R. & Rast, W.) 1–16 (Springer, 2011).
31. Schachtman, D. P., Reid, R. J. & Ayling, S. M. Phosphorus Uptake by Plants: From Soil to Cell. *Plant Physiol.* **116**, 447, https://doi.org/10.1104/pp.116.2.447 (1998).
32. Polizzotto, M. L., Kocar, B. D., Benner, S. G., Sampson, M. & Fendorf, S. Near-surface wetland sediments as a source of arsenic release to ground water in Asia. *Nature* **454**, 505–508, https://doi.org/10.1038/nature07093 (2008).
33. Fendorf, S., Michael, H. A. & van Geen, A. Spatial and temporal variations of groundwater arsenic in South and Southeast Asia. *Science* **328**, 1123–1127, https://doi.org/10.1126/science.1172974 (2010).
34. Flora, S. J. S. In *Handbook of arsenic toxicology* 1st Editon, 1–49 (Academic Press, 2015).
35. Kato, L. S., De Nadai Fernandes, E. A., Raab, A., Bacchi, M. A. & Feldmann, J. Arsenic and cadmium contents in Brazilian rice from different origins can vary more than two orders of magnitude. *Food Chem.* **286**, 644–650, https://doi.org/10.1016/j.foodchem.2019.02.043 (2019).
36. Shi, G. L. *et al*. Accumulation and distribution of arsenic and cadmium in winter wheat (*Triticum aestivum L.*) at different developmental stages. *Sci. Total Environ.* **667**, 532–539, https://doi.org/10.1016/j.scitotenv.2019.02.394 (2019).
37. Schaller, J., Wang, J., Islam, M. R. & Planer-Friedrich, B. Black carbon yields highest nutrient and lowest arsenic release when using rice residuals in paddy soils. *Sci. Rep.* **8**, 17004, https://doi.org/10.1038/s41598-018-35414-3 (2018).
38. Signes-Pastor, A. J. *et al*. Infants' dietary arsenic exposure during transition to solid food. *Sci. Rep.* **8**, 7114, https://doi.org/10.1038/s41598-018-25372-1 (2018).

39. Ritchie, R. J. & Mekjinda, N. Arsenic toxicity in the water weed *Wolffia arrhiza* measured using Pulse Amplitude Modulation Fluorometry (PAM) measurements of photosynthesis. *Ecotoxicol. Environ. Saf.* **132**, 178–185, https://doi.org/10.1016/j.ecoenv.2016.06.004 (2016).
40. Khaska, S., Le Gal La Salle, C., Sassine, L., Bruguier, O. & Roig, B. Innovative isotopic method to evaluate bioaccumulation of As and MTEs in *Vitis vinifera*. *Sci. Total Environ.* **651**, 1126–1136, https://doi.org/10.1016/j.scitotenv.2018.09.222 (2019).
41. Taylor, V. F. *et al.* Distinct arsenic metabolites following seaweed consumption in humans. *Sci. Rep.* **7**, 3920, https://doi.org/10.1038/s41598-017-03883-7 (2017).
42. Mitsukawa, N. *et al.* Overexpression of an *Arabidopsis thaliana* high-affinity phosphate transporter gene in tobacco cultured cells enhances cell growth under phosphate-limited conditions. *Proc. Natl. Acad. Sci. USA* **94**, 7098–7102, https://doi.org/10.1073/pnas.94.13.7098 (1997).
43. Nussaume, L. *et al.* Phosphate import in plants: focus on the *PHT1* transporters. *Front. Plant Sci.* **2**, 83, https://doi.org/10.3389/fpls.2011.00083 (2011).
44. Peñaloza, E. *et al.* Characterization of the high-affinity phosphate transporter *PHT1;4* gene promoter of *Arabidopsis thaliana* in transgenic wheat. *Biol. Plant.* **61**, 453–462, https://doi.org/10.1007/s10535-016-0672-9 (2016).
45. Pradhan Mitra, P. & Loqué, D. Histochemical staining of *Arabidopsis thaliana* secondary cell wall elements. *J. Vis. Exp.*, 51381, https://doi.org/10.3791/51381 (2014).
46. Mukherjee, P. *et al.* Live imaging of inorganic phosphate in plants with cellular and subcellular resolution. *Plant Physiol.* **167**, 628–638, https://doi.org/10.1104/pp.114.254003 (2015).
47. Catarecha, P. *et al.* A mutant of the *Arabidopsis* phosphate transporter *PHT1;1* displays enhanced arsenic accumulation. *Plant Cell* **19**, 1123–1133, https://doi.org/10.1105/tpc.106.041871 (2007).
48. Ojida, A., Mito-oka, Y., Sada, K. & Hamachi, I. Molecular recognition and fluorescence sensing of monophosphorylated peptides in aqueous solution by bis(zinc(II)-dipicolylamine)-based artificial receptors. *J. Am. Chem. Soc.* **126**, 2454–2463, https://doi.org/10.1021/ja038277x (2004).

Acknowledgements

This research was supported by the Faculty of Science, Mahidol University and the Thailand Research Fund (IRG5980001). NM is grateful to RGJ Ph.D. Programme (PHD/1086/2557). Yoshifumi Miyahara is grateful for the original synthesis of the Dpa-Zn^{II} library compounds.

Author contributions

J.W. and A.O. designed the project; S.P. and V.R. conducted the computational molecular modeling; N.M., J.W. and A.O. performed the experiments and analyzed the results; N.M. and J.W. wrote the manuscript; N.M., R.J.R., I.H., A.O. and J.W. contributed to the improvement of project and revised the manuscript.

Competing interests

The authors declare no competing interests.

Additional information

Supplementary information is available for this paper at https://doi.org/10.1038/s41598-020-59585-0.

Correspondence and requests for materials should be addressed to A.O. or J.W.

Reprints and permissions information is available at www.nature.com/reprints.

Publisher's note Springer Nature remains neutral with regard to jurisdictional claims in published maps and institutional affiliations.